Solitons and vortices in two-dimensional discrete nonlinear Schrödinger systems with spatially modulated nonlinearity

P. G. Kevrekidis
Department of Mathematics and Statistics, University of Massachusetts, Amherst, Massachusetts 01003-4515, USA
and Center for Nonlinear Studies and Theoretical Division, Los Alamos National Laboratory, Los Alamos, New Mexico 87545, USA

Boris A. Malomed
Department of Physical Electronics, School of Electrical Engineering, Faculty of Engineering, Tel Aviv University, Tel Aviv 69978, Israel

Avadh Saxena and A. R. Bishop
Center for Nonlinear Studies and Theoretical Division, Los Alamos National Laboratory, Los Alamos, New Mexico 87545, USA

D. J. Frantzeskakis
Department of Physics, University of Athens, Panepistimiopolis, Zografos, Athens 15784, Greece
(Received 15 December 2014; published 7 April 2015)

We consider a two-dimensional (2D) generalization of a recently proposed model [Gligorić *et al.*, Phys. Rev. E **88**, 032905 (2013)], which gives rise to bright discrete solitons supported by the defocusing nonlinearity whose local strength grows from the center to the periphery. We explore the 2D model starting from the anticontinuum (AC) limit of vanishing coupling. In this limit, we can construct a wide variety of solutions including not only single-site excitations, but also dipole and quadrupole ones. Additionally, two separate families of solutions are explored: the usual "extended" unstaggered bright solitons, in which all sites are excited in the AC limit, with the same sign across the lattice (they represent the most robust states supported by the lattice, their 1D counterparts being those considered as 1D bright solitons in the above-mentioned work), and the vortex cross, which is specific to the 2D setting. For all the existing states, we explore their stability (also analytically, when possible). Typical scenarios of instability development are exhibited through direct simulations.

DOI: 10.1103/PhysRevE.91.043201 PACS number(s): 05.45.Yv, 03.75.Lm, 42.65.Tg

I. INTRODUCTION

In the past few years, a topic that has drawn an ever-increasing amount of interest in the realm of physical systems modeled by nonlinear-Schrödinger (NLS) type equations concerns the examination of solitary waves and their existence, stability, and dynamical properties in the presence of spatially inhomogeneous nonlinearities. A review which covers many aspects of this topic can be found in Ref. [1]. A ramification that is gaining attention within this broader theme concerns the possibility of the existence of bright coherent structures in the context of *defocusing* nonlinearities. As is well known [2–4], systems with a self-defocusing nonlinearity support wave excitations in the form of dark solitons, vortices, vortex rings, etc., i.e., structures supported by a nonvanishing background at infinity. However, a fundamental proposal, put forth a few years ago [5–8], was that, if the local strength of the self-defocusing nonlinearity in the D-dimensional space grows with distance r from the center at any rate faster than r^D, then bright solitary waves and vortical structures can self-trap within such settings. Subsequently, this class of models was extended to include spatially inhomogeneous nonlinear losses [9], higher-power (e.g., quintic) nonlinearities [10], other wave forms such as domain walls [11], as well as settings related to Fermi and Bose gases [12], dipolar Bose-Einstein condensates (BECs) [13], nonlocal media [14], discrete systems [15], and complex three-dimensional (3D) topological patterns [16]. Most recently, the Bose-Hubbard model with the same type of spatial modulation of the self-repulsive nonlinearity was introduced, and existence of the corresponding quantum discrete solitons was demonstrated in [17].

Another area which has drawn major interest over the past two decades is the study of models based on the discrete NLS (DNLS) equation [18]. DNLS systems have been serving not only as fundamental dispersive systems combining nonlinearity and discreteness, but also as models suitable for the direct description of dynamics in arrays of optical waveguides [19,20] and atomic BECs loaded into optical lattices [21]. There are numerous other applications of DNLS models, ranging from their use as envelope equations for understanding the denaturation of the DNA double strand [22], and the localization of energy in granular crystals [23,24], to the dynamics of protein loops [25].

Our aim in the present work is to combine these two important directions by extending the one-dimensional (1D) model and analysis presented in a recent work [15] to two-dimensional (2D) lattices. We will also develop a different approach, examining the problem from the perspective of the well-established anticontinuum (AC) limit [26], which offers two important advantages. On the one hand, in the AC limit, which corresponds to vanishing coupling between the nearest neighbors, we are able to construct solutions systematically, by initially exciting a single site, multiple sites (two for dipole configurations, or four for quadrupole ones), as well as possibly all sites in what we refer to as an extended solution. The same approach allows one to produce not only real wave forms (with relative phases 0 or π between adjacent sites), but also complex ones, such as discrete vortices. The latter,

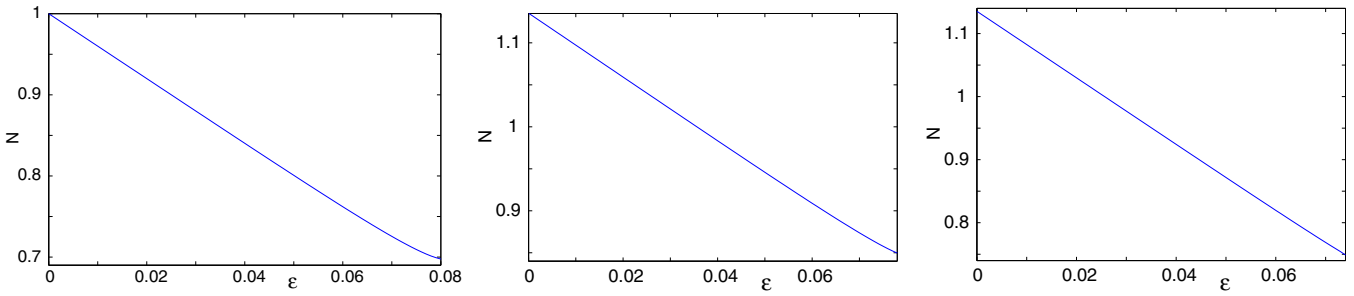

FIG. 1. (Color online) Numerically generated dependencies $N(\epsilon)$ for the families of single-site, in-phase two-site, and out-of-phase two-site modes are shown in the left, middle, and right panels, respectively.

have not only been theoretically proposed [27,28], but also experimentally observed in photorefractive crystals consistent with the theoretical prediction [29,30]. The second important advantage is that, following the methodology of Refs. [31,32], we are able to provide a systematic classification of the spectral stability of the states, while departing from the AC limit. In this way, we are able to predict which states are robust near this limit. We also numerically corroborate these predictions and, finally, we use direct simulations to explore the outcome of the evolution of unstable states.

The presentation of the paper is structured as follows. In Sec. II, we introduce the model and present the theoretical analysis of the existence and stability of different states. In Sec. III, we explore the model in terms of the numerically implemented bifurcation theory (as concerns the existence and spectral stability of the examined states), and report results of direct simulations of unstable states. In Sec. IV, we summarize our findings and discuss directions for future research.

II. THE MODEL AND ITS ANALYSIS

Generalizing to 2D the considerations of Ref. [15], we consider a DNLS model of the following general form:

$$i\dot{u}_{m,n} = -\varepsilon(u_{m,n-1} + u_{m,n+1} + u_{m+1,n} + u_{m-1,n} - 4u_{m,n}) + g(m,n)|u_{m,n}|^2 u_{m,n}, \tag{1}$$

where ε accounts for the coupling between adjacent wells, and $g(m,n)$ represents the local strength of the nonlinearity. Prototypical examples represent arrays of waveguides in the nonlinear optical material $LiNbO_3$ [33–35] and atomic BECs (e.g., of ^{87}Rb or ^{23}Na gases) confined in an optical lattice in the superfluid regime [36,37]. As argued in Ref. [1], a local modulation of the Kerr coefficient in optics, or a spatial modulation of the scattering length in atomic BECs (via the Feshbach resonance) straightforwardly leads to settings of the type we consider here.

In the present section, we develop the analysis in the general form. For the numerical investigation of Sec. III, we resort to a specific form of the spatial modulation,

$$g(m,n) = \exp[2(|m| + |n|)], \tag{2}$$

which is a counterpart of the 1D modulation adopted in Ref. [15]. We will also often compare our findings to those in the homogeneous lattice with $g(m,n) = 1$, where solely *staggered* solitary modes [18] can be obtained for the presently considered nonlinearity of the defocusing sign.

Our first aim is to construct stationary states in the form of $u_{m,n} = e^{-i\mu t} v_{m,n}$ with chemical potential (in the BEC context) $\mu > 0$, which leads to an equation for $v_{m,n}$:

$$\mu v_{m,n} = -\varepsilon \Delta_2 v_{m,n} + g(m,n)|v_{m,n}|^2 v_{m,n}, \tag{3}$$

with $\Delta_2 v_{m,n} \equiv v_{m,n-1} + v_{m,n+1} + v_{m+1,n} + v_{m-1,n} - 4v_{m,n}$. The total norm of the mode is defined in the usual form,

$$N = \sum_{m,n} |u_{m,n}|^2, \tag{4}$$

and is a conserved quantity of the model. Families of stationary solutions are characterized below by dependencies $N(\varepsilon)$ for $\mu \equiv 1$ (see Fig. 1). It is also possible to cast these dependencies into the form of $N(\mu)$ for $\varepsilon \equiv 1$: as follows from Eqs. (3) and (4), obvious rescaling yields

$$N(\varepsilon,\mu) = \varepsilon N(1,\mu/\varepsilon) = \mu N(\varepsilon/\mu,1). \tag{5}$$

Applying this for $\varepsilon = 1$, we obtain $N(1,\mu) = \mu N(1/\mu,1)$. In this connection, it is relevant to mention that a necessary stability condition for solitary modes supported by repulsive nonlinearities is given by the anti-Vakhitov-Kolokolov criterion [38], $dN/d\mu > 0$. In particular, nearly linear dependencies of N on ε observed in Fig. 1, if substituted into Eq. (5), correspond to $dN/d\mu \approx N(\varepsilon = 0,\mu) > 0$. Indeed, actual results for the stability reported below confirm that the particular instability mechanism, which might be detected by the anti-Vakhitov-Kolokolov criterion, is absent in the present system.

The starting point of the analysis is the AC limit of $\varepsilon = 0$, corresponding to the case where the sites get decoupled. In this limit, the only local solutions corresponding, respectively, to nonexcited or excited sites, are $v_{m,n} = 0$ or

$$v_{m,n} = \sqrt{\mu/g(m,n)}\, e^{i\theta_{m,n}}. \tag{6}$$

Equation (6) yields, in fact, the Thomas-Fermi approximation (TFA) for the lattice field [8,15], which, in particular, leads to the conclusion that the solution is normalizable (in other words, it is a physically relevant one), i.e., its norm (4) converges, under the condition that $g(m,n)$ must grow, as $|m|,|n| \to \infty$, at any rate faster than $(m^2 + n^2)$.

Based on this AC-limit solution, we can choose to excite any configuration in the AC limit, with an arbitrary phase pattern. The actual issue is which of these configurations persist at finite values of intersite coupling ε. To address it, works [31,32,39] (for 1D, 2D, and 3D cubic lattices, respectively)

have developed a "persistence condition," which we now adapt to the present setting.

Suppose that a string of three sites is excited, with coordinates $(m,n-1)$, (m,n), and $(m,n+1)$. Then the persistence condition, adapted to the present setting, reads

$$\frac{\sin(\theta_{m,n}-\theta_{m,n-1})}{\sqrt{g(m,n)g(m,n-1)}}=\frac{\sin(\theta_{m,n+1}-\theta_{m,n})}{\sqrt{g(m,n+1)g(m,n)}}. \tag{7}$$

Pertaining to two-point functions defined for adjacent pairs of sites, it can be generalized for any set of such pairs of sites.

In 1D, given that this set of two-point functions is the same for all sites up to $\pm\infty$, for solutions that vanish at infinity, the persistence condition allows only configurations with relative phases 0 or π. However, this is no longer the case in 2D, as the condition can be satisfied over closed contours without the need to extend the considerations to infinity. As a result, in the latter setting complex configurations, including vortices, are possible. Nevertheless, the simpler configurations are the ones with relative phases $\Delta\theta_n=0$ or π, which we predominantly consider below.

Particular configurations that we aim to study are the following:

(1) A single-site solution with $v_{0,0}=\sqrt{\mu/g(0,0)}$ and vanishing amplitude at all other sites.

(2) A "dipolar" state residing on a pair of sites, e.g., (0,0) and (1,0). These two sites may be excited *in* or *out* of phase.

(3) "Quadrupole" configurations supported by four sites. Although additional structures can also be considered (which is also true for the dipolar modes), we restrict our considerations here to the square-shaped set of four sites (0,0), (1,0), (1,1), (0,1). Qualitative conclusions that we will infer for the stability will not be different if we choose another quartet of sites, although details may differ.

(4) We also consider the extended unstaggered solution in which *all* sites of the lattice are excited with the same sign, as $v_{m,n}=\sqrt{\mu/g(m,n)}$ [see Eq. (6)]. Actually, the 1D counterpart of such a state was the subject of the analysis in Ref. [15], while solutions which amount to single- or few-site excitations in the AC limit were not considered in that work.

(5) Finally, while for the above-mentioned square-shaped quartet of sites, (0,0), (1,0), (1,1), (0,1), with $g(m,n)$ taken even in both n and m, we were unable to continue vortical solutions for finite ε, we were able to do so for a cross-shaped quartet, (1,0), (0,1), (−1,0), (0, −1), which features an empty site at the center. This (failure to continue the above-mentioned "vortex square" configuration) is perhaps rather natural to expect on the basis of the symmetry of our $g(m,n)$ profile in Eq. (2) which is symmetric under parity, while the above square is not; instead, the vortex cross is. However, if we try a spatial modulation of the nonlinear prefactor in the form

$$g(m,n)=\exp[2(|m-0.5|+|n-0.5|)], \tag{8}$$

then clearly the symmetry of the vortex square around (0.5,0.5) is consonant with that of $g(m,n)$ and as we will illustrate below the vortex square configuration can also be continued to finite ε in that setting.

Now, we turn to the consideration of the stability of the discrete configurations. To this end, we employ the usual linearization ansatz for perturbations with small amplitude δ:

$$u_{m,n}=e^{-i\mu t}[v_{m,n}+\delta e^{\lambda t}p_{m,n}+\delta e^{\lambda^\star t}q^\star_{m,n}], \tag{9}$$

(where * denotes complex conjugate) and derive equations at order $O(\delta)$ for $(p_{m,n},q_{m,n})$. For simplicity, we mention here only the ensuing eigenvalue problem in the case when the unperturbed solution $v_{m,n}$ is real, also using the decomposition [31] $p_{m,n}=a_{m,n}+ib_{m,n}$ and $q_{m,n}=a_{m,n}-ib_{m,n}$,

$$\lambda\begin{pmatrix}a_{m,n}\\ b_{m,n}\end{pmatrix}=\begin{pmatrix}0 & \mathcal{L}_-\\ -\mathcal{L}_+ & 0\end{pmatrix}\begin{pmatrix}a_{m,n}\\ b_{m,n}\end{pmatrix}. \tag{10}$$

In these expressions the linear operators are defined as follows: $\mathcal{L}_-b_{m,n}=-\varepsilon\Delta_2 b_{m,n}-\mu b_{m,n}+g(m,n)v^2_{m,n}b_{m,n}$ and $\mathcal{L}_+a_{m,n}=-\varepsilon\Delta_2 a_{m,n}-\mu a_{m,n}+3g(m,n)v^2_{m,n}a_{m,n}$. Rewriting the above non-self-adjoint eigenvalue problem as a combined fourth-order one, we obtain

$$\lambda^2 b_{m,n}=-\mathcal{L}_+\mathcal{L}_-b_{m,n}\Rightarrow\lambda^2\mathcal{L}_+^{-1}b_{m,n}=-\mathcal{L}_-b_{m,n}. \tag{11}$$

It is relevant now to point out that near the AC limit of $\varepsilon\to 0$, $\mathcal{L}_+$ becomes a multiplicative operator with positive entries, which is obviously invertible. Forming the inner product of Eq. (11) with $b_{m,n}$, we obtain

$$\lambda^2=-\frac{\langle b_{m,n},\mathcal{L}_-b_{m,n}\rangle}{\langle b_{m,n},\mathcal{L}_+^{-1}b_{m,n}\rangle}, \tag{12}$$

where $\langle,\rangle$ denotes the standard inner product. Given the multiplicative nature of $\mathcal{L}_+$ in the AC limit, the leading-order approximation near $\varepsilon=0$ yields $\mathcal{L}_+^{-1}\to(2\mu)^{-1}$ for excited sites with $v_{m,n}\neq 0$ [and $\mathcal{L}_+^{-1}\to-(\mu)^{-1}$ for the nonexcited ones]. Thus, eigenvalues of the above-mentioned real solutions are directly associated with the operator $\mathcal{L}_-$, up to the above-mentioned multiplicative factor -2μ (henceforth, without loss of generality, we will set $\mu=1$).

It is straightforward to see that for all the nonexcited sites with $v_{m,n}=0$, $\mathcal{L}_-=-1$, $\lambda=\pm i$. These eigenvalues will form, as ε becomes nonzero, the continuous spectrum which, in the 2D setting, corresponds to the interval $\pm i[1-8\varepsilon,1]$. On the other hand, the eigenvalues that may lead to instability (at least for small ε) are those stemming from the excited sites for which $\mathcal{L}_-$ vanishes to the leading order, hence these eigenvalues are $\lambda=0$ at $\varepsilon=0$. In principle, these eigenvalue pairs may become real immediately as ε becomes nonzero. It is then of critical importance, as regards the stability, to identify eigenvalues of the matrix $M=\langle b,\mathcal{L}_-b\rangle\equiv\varepsilon\mathcal{M}$. Upon obtaining eigenvalues γ of the matrix $\mathcal{M}$, based on the theory presented in Refs. [31,32,39] (see also [18]) and the above exposition, the eigenvalues λ of the full problem will be given, in view of Eq. (12), by $\lambda=\pm\sqrt{-2\varepsilon\gamma}$. We perform this calculation below for two- and four-site real excitations. For the single-site excitation, there is only one pair at $\lambda=0$. Actually, for all configurations one pair always remains at the origin, due to the phase (gauge) invariance of the model (in the case of the single-site excitation, it is the sole one, so there is no bifurcation occurring). For the extended solution, since all sites are excited, the number of pairs of eigenvalues at the origin is equal to the number of nodes in the lattice, hence the corresponding matrix $\mathcal{M}$ also has the same number of rows and columns. Finally, for the only genuinely complex configuration considered here, the computation of matrix $\mathcal{M}$

is considerably more complicated, as it should be performed at a higher order [$O(\varepsilon^2)$, rather than $O(\varepsilon)$, as the relevant excited sites are two lattice spacings apart and only couple at $O(\varepsilon^2)$]. We do not present details of that calculation here.

In the case of two-site excitations, the matrix $\mathcal{M}$ can be computed explicitly [upon calculating the leading order i.e., an $O(\varepsilon)$ correction to the solution] as

$$\mathcal{M} = \begin{pmatrix} \sqrt{\frac{g(m,n)}{g(m,n+1)}} & -1 \\ -1 & \sqrt{\frac{g(m,n+1)}{g(m,n)}} \end{pmatrix} \cos(\theta_{m,n+1} - \theta_{m,n}). \quad (13)$$

Here, we assume that the two excited sites are (m,n) and $(m,n+1)$. The eigenvalues are then $\gamma = 0$ and $\gamma = c\cos(\theta_{m,n+1} - \theta_{m,n})$, where

$$c \equiv \sqrt{\frac{g(m,n)}{g(m,n+1)}} + \sqrt{\frac{g(m,n+1)}{g(m,n)}}. \quad (14)$$

One of them, as indicated above, remains at the origin, while the other grows along the real axis for out-of-phase excitations (making these immediately unstable when ε becomes nonzero) or along the imaginary axis for in-phase excitations, which does not lead to immediate destabilization. In both cases, note that the inequality $c \geqslant 2$ leads to a growth rate for these eigenvalues which is larger than that of the homogeneous limit of constant $g(m,n) = 1$. Furthermore, even for the in-phase mode, which is stable for small ε, as the respective imaginary eigenvalues grow according to $\lambda = \pm i\sqrt{2c\varepsilon}$ [recall c is defined by Eq. (14)], they eventually collide with the edge of the above-mentioned continuous spectrum, at $\pm i(1-8\varepsilon)$, leading to an oscillatory-instability threshold, $\varepsilon = (1/64)(8 + c - \sqrt{c^2 + 16c})$. Given the larger growth rate of the imaginary eigenvalue pair bifurcating from the origin, this instability occurs at smaller values of ε in comparison to the homogeneous limit of $c = 2$.

We now turn to the four-excited-site case, which is considerably more complicated. Here, the reduced matrix $\mathcal{M}$ is of size 4×4. Labeling the relative phase factors as $r_{10} = \cos(\theta_{1,0} - \theta_{0,0})$, $r_{21} = \cos(\theta_{1,1} - \theta_{1,0})$, $r_{32} = \cos(\theta_{0,1} - \theta_{1,1})$, and $r_{03} = \cos(\theta_{0,0} - \theta_{0,1})$, we can write the matrix

$$\mathcal{M} = \begin{pmatrix} \sqrt{\frac{g(0,0)}{g(1,0)}}r_{10} + \sqrt{\frac{g(0,0)}{g(0,1)}}r_{03} & -r_{10} & 0 & -r_{03} \\ -r_{10} & \sqrt{\frac{g(1,0)}{g(0,0)}}r_{10} + \sqrt{\frac{g(1,0)}{g(1,1)}}r_{21} & -r_{21} & 0 \\ 0 & -r_{21} & \sqrt{\frac{g(1,1)}{g(1,0)}}r_{21} + \sqrt{\frac{g(1,1)}{g(0,1)}}r_{32} & -r_{32} \\ -r_{03} & 0 & -r_{32} & \sqrt{\frac{g(0,1)}{g(1,1)}}r_{32} + \sqrt{\frac{g(0,1)}{g(0,0)}}r_{03} \end{pmatrix}. \quad (15)$$

This matrix has a single zero eigenvalue. Furthermore, if all r's are positive, then the eigenvalues γ are also positive, hence the eigenvalues of the full problem are imaginary at $\varepsilon > 0$. On the other hand, if one (or more) of the relative phase factors r is (are) negative, then the corresponding number of negative γ's emerge, leading to pairs of real eigenvalues, and hence instability of the configuration. These features are directly in line with what is known for the homogeneous defocusing model (see, e.g., Ref. [40]). They are also the reverse of the focusing nonlinearity case (i.e., the features corresponding to negative r in one case correspond to those for positive r in the other). While, in principle, the eigenvalues of this 4×4 matrix can be obtained in an explicit analytical form, the expressions are too cumbersome to be useful. Therefore, below we turn to numerical computations, comparing the results with those of the above analysis, whenever possible.

III. NUMERICAL RESULTS

A. Stationary modes and their stability

In our numerical analysis, we first explore branches of stationary states and their stability, and then proceed to simulations of the evolution of perturbed solutions. The first localized state we consider in the AC limit is the single-site one. This solution family is characterized by the dependence of the norm of Eq. (4) on the coupling constant ε, which is displayed in the left panel of Fig. 1 (the nearly linear shapes of the dependencies observed in this figure are explained by the small size of the respective range of ε). Principal eigenvalues associated with this branch, as well as a typical example of its profile (for $\varepsilon = 0.08$), are shown in Fig. 2. As indicated in the previous section, throughout its existence region, this branch is stable, with a single pair of eigenvalues at the origin. For this branch, multiple pairs of eigenvalues bifurcate from the edge of the continuous-spectrum band, $\lambda = \pm(1-8\varepsilon)i$: the first one bifurcates around $\varepsilon = 0.055$, and the branch cannot be continued past $\varepsilon = 0.082$. It can be clearly seen from its profile close to this termination point that it collides with a branch bearing a positive excitation at the central site and a negative excitation at adjacent ones.

The next two branches we examine correspond to two-site excitations. The in-phase and out-of-phase ones are shown by the middle and right panels of Fig. 1, and by Figs. 3 and 4. In the former case, the eigenvalue bifurcating from the origin is approximately $\pm 2.484\sqrt{\varepsilon}i$. It collides with the band edge, $\pm(1-8\varepsilon)i$ at $\varepsilon = 0.053$ or 0.052, according to the analytical approximation and numerical results, respectively, which demonstrates a very good agreement between the two in the prediction of the threshold for the oscillatory instability arising for this branch, as well as for the entire ε dependence of the eigenvalue pair. In Fig. 3 we also show, by means of the lower (magenta) curve, $\mathrm{Im}(\lambda) = \pm 2\sqrt{\varepsilon}$, the analytical prediction for the homogeneous system, with $g(m,n) = 1$. We note that in the inhomogeneous model the eigenvalue pair grows more rapidly, thus leading to an instability at a lower value of the coupling, than for its homogeneous counterpart. The branch is unstable past the point of $\varepsilon = 0.052$, and for $\varepsilon > 0.065$ further eigenvalue pairs bifurcate off of the

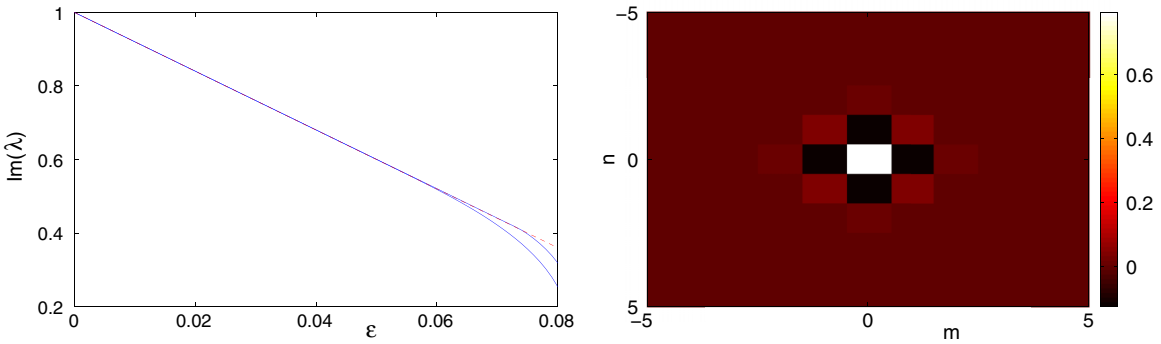

FIG. 2. (Color online) The branch corresponding to the single-site excitation. The left panel shows eigenvalues bifurcating from the edge of the continuous spectrum band (the first around $\varepsilon = 0.055$ and two more at a slightly larger value of ε), rapidly approaching the spectral-plane's origin as $\varepsilon \to 0.082$, the value at which the present branch terminates. Here and in similar plots displayed below, the dependence of the edge of the continuous wave band on ε, $\lambda = \pm(1 - 8\varepsilon)i$, is shown by the red dashed line. The right panel shows the profile of the branch at $\varepsilon = 0.08$.

continuous spectrum, their collision with the origin leading to the termination of the branch at larger values of ε; in the right panel of the figure, the branch is shown for $\varepsilon = 0.079$.

In the case of the out-of-phase two-site excitation, as seen in Fig. 4, the linearization around the solution produces a real eigenvalue pair predicted to be $\lambda = \pm 2.484\sqrt{\varepsilon}$, which is reasonably accurate for small ε. For larger values of ε, higher-order terms apparently take over, pulling the eigenvalue back to the origin (nevertheless, the instability is present at all the values of ε that we considered). A typical example of the profile of the discrete mode is shown in the right panel of Fig. 4 for $\varepsilon = 0.07$. The profile suggests that the solution collides with the single-site one, and with the above-mentioned cross-shaped solution with four negatively excited sites around the central one. Therefore, the present mode represents one of the four asymmetric branches—the other three arise by rotating the present one by $\pi/2$, π, and $3\pi/2$ (see the right panel of Fig. 4)—which are generated by a pitchfork bifurcation.

Examining now the four-site excitations in the framework of the analysis based on Eq. (15), we conclude that asymmetric configurations always bear a number of instabilities. [By "asymmetric" here, we mean configurations other than the in-phase one, in which all phases of the four excited sites are the same, e.g., (0,0,0,0), and the out-of-phase one, in which the phases alternate between 0 and π, e.g., $(0,\pi,0,\pi)$ for the four sites of the square. Any other phase combination, e.g., $(0,\pi,\pi,0)$, $(0,0,\pi,0)$, etc., is considered asymmetric.] For demonstration purposes, we restrict our considerations here to the two most symmetric examples, namely, the in-phase state shown in Fig. 5, and the out-of-phase one in Fig. 6. In the case of the four-site, in-phase excitation, there are three eigenvalue pairs bifurcating from the spectral-plane's origin, whose behavior is determined by Eq. (15). One of the three pairs is predicted to have eigenvalues $\lambda = \pm 3.513\sqrt{\varepsilon}i$, and two others to have $\lambda = \pm 2.484\sqrt{\varepsilon}i$. As a result, by setting these eigenvalues equal to the edge of the continuous-spectrum band, $(1 - 8\varepsilon)i$, we can predict the onset of instabilities at $\varepsilon = 0.0386$ (the first one), and at $\varepsilon = 0.053$ (a pair of additional ones). Numerically these instabilities are found to occur, respectively, at $\varepsilon = 0.036$ and at $\varepsilon = 0.053$, in very good agreement with the theoretical predictions. Generally, in the present case of the four-site modes, we again observe good agreement between the analytical predictions for the eigenvalues and their numerical counterparts. In addition, we point out that here, too, the eigenvalues move more rapidly along the imaginary axis than their counterparts in the homogeneous model (shown by magenta dash-dotted lines in Fig. 5). The configuration is generically unstable for $\varepsilon > 0.036$, and a typical example of this mode is shown for $\varepsilon = 0.075$ in the right panel of the figure.

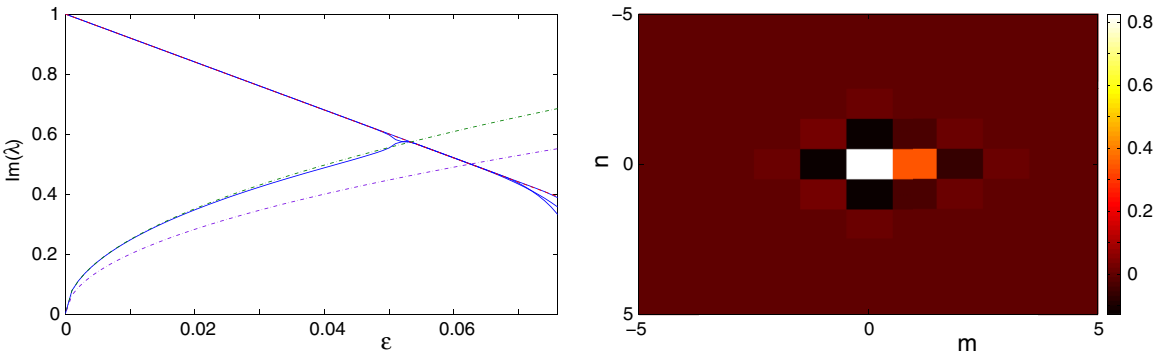

FIG. 3. (Color online) In-phase configuration: the left panel shows the imaginary eigenvalue growing from the origin, as per numerical results (blue solid line), according to the analytical prediction (green dash-dotted line), and in the homogeneous model (the lower dash-dotted line, also obtained in an analytical form). Eigenvalues bifurcating from the edge of the continuous-spectrum band are also shown by blue solid lines. The right panel displays an example of this wave form for $\varepsilon = 0.079$.

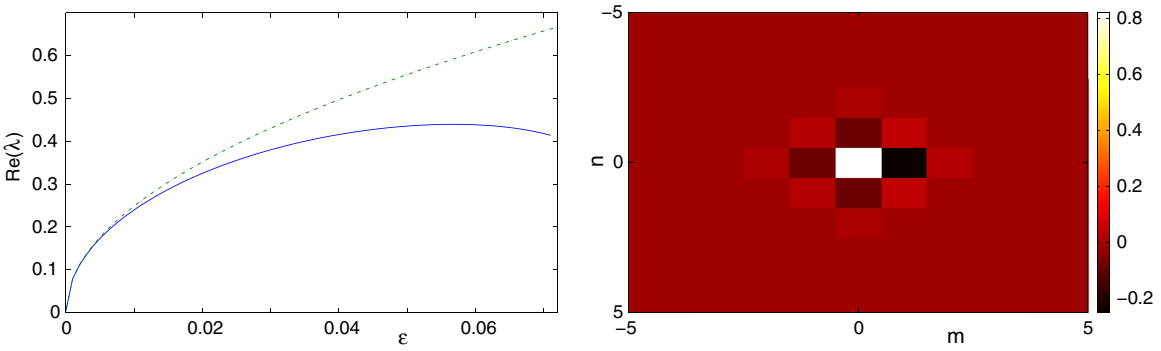

FIG. 4. (Color online) Similar to the previous graph but for the out-of-phase configuration. In this case, however, the eigenvalue pair bifurcating from the origin moves to the real line and hence the real part of the relevant eigenvalue is shown (blue solid line: numerical linear stability result; green dash-dotted line: theory). The right panel shows the corresponding wave form for $\varepsilon = 0.07$.

In the case of the four-site, out-of-phase (between adjacent sites) excitation, the analysis produces three real eigenvalue pairs, bifurcating from the origin as ε increases. The dominant one is predicted to be $\lambda = \pm 3.513\sqrt{\varepsilon}$, while two more correspond to $\lambda = \pm 2.484\sqrt{\varepsilon}$. Here again, as is typical for configurations with real eigenvalue pairs, the agreement between the analytical prediction and numerical results is good for small coupling strengths, but progressively deteriorates as the coupling grows. The state is found to be unstable for all values of the coupling. A typical example of the state for $\varepsilon = 0.055$ is shown in the right panel of Fig. 6.

We now turn to the examination of a genuinely complex state, namely, of the discrete "vortex cross" (see Fig. 7). While we were able to identify and continue this type of state in the symmetric pattern illustrated in the figure, it is worth noting that when we attempted to construct a similar configuration based on the square of the four-site excitations shown in Figs. 5 and 6, we were unable to continue it to finite couplings; however, see also the discussion below.

In the case of the vortex crosses of Fig. 7, there are three eigenvalue pairs that bifurcate from the origin along the imaginary axis, attesting to the stability of the structure for small ε. Importantly, these eigenvalues scale as $\propto \varepsilon$, rather than $\sqrt{\varepsilon}$, and can only be captured at the second order of perturbation theory, which is not considered here. As these eigenvalue pairs move along the imaginary axis, further pairs bifurcate from the edge of the continuous-spectrum band at $\lambda = \pm(1 - 8\varepsilon)i$, starting at approximately $\varepsilon = 0.05$. As ε increases, these pairs approach each other and eventually collide around $\varepsilon = 0.068$ (shown in the right panels of Fig. 7), rendering the branch of solutions unstable past this critical point. This happens because collisions of the former eigenvalue pair, bifurcating from 0, with the latter one, which bifurcates from the band edge, give rise to complex quartets and oscillatory instabilities.

As indicated in Sec. II (and also above) a vortex square profile over the sites (0,0), (1,0), (1,1), and (0,1) is not possible to continue to finite ε in the case of the parity symmetric nonlinear prefactor profile of Eq. (2). However, when we considered the modified profile of Eq. (8) which is symmetric around (0.5,0.5), as is the above "vortex square," we were indeed able to continue the vortex square configuration to a finite coupling ε, as well as to monitor its stability. In fact, such a solution turns out to be stable up to $\varepsilon \approx 0.08$ and is thus fairly robust. Moreover, similar to the vortex cross, it appears to have two (eventually splitting) pairs of nearly linear (in their dependence on ε) eigenvalues and one which grows with a higher power of ε, along the positive imaginary axis. It is eventually the collision of these eigenvalues with ones arising from the continuous spectrum that leads to the instability of the solution for sufficiently large ε. These features are illustrated in Fig. 8, by analogy with the vortex cross characteristics of Fig. 7.

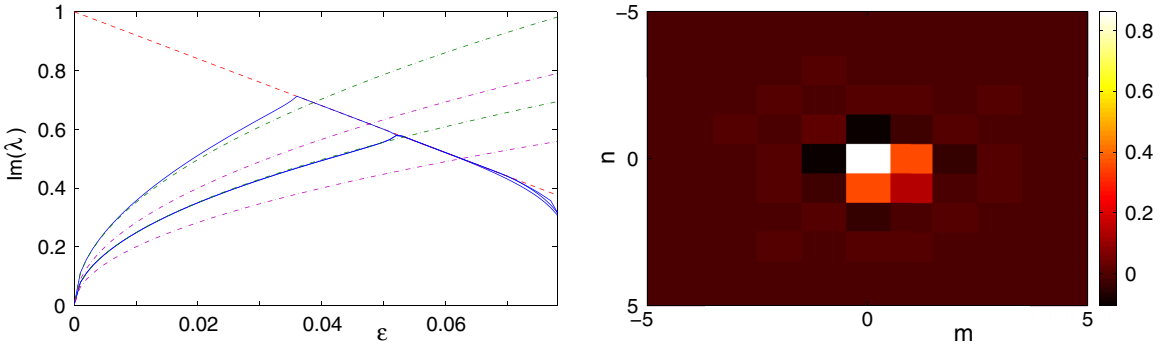

FIG. 5. (Color online) Four-site, in-phase excitation: In the left panel of the figure three pairs of imaginary eigenvalues bifurcating from the origin are shown by the blue solid line (the lower parabolic line corresponds to a double pair). The corresponding analytical prediction is shown by the green dash-dotted line, while the prediction for the homogeneous model is presented by the magenta dash-dotted line. The edge of the continuous-spectrum band is shown by the red dashed line. The right panel shows the configuration for $\varepsilon = 0.075$.

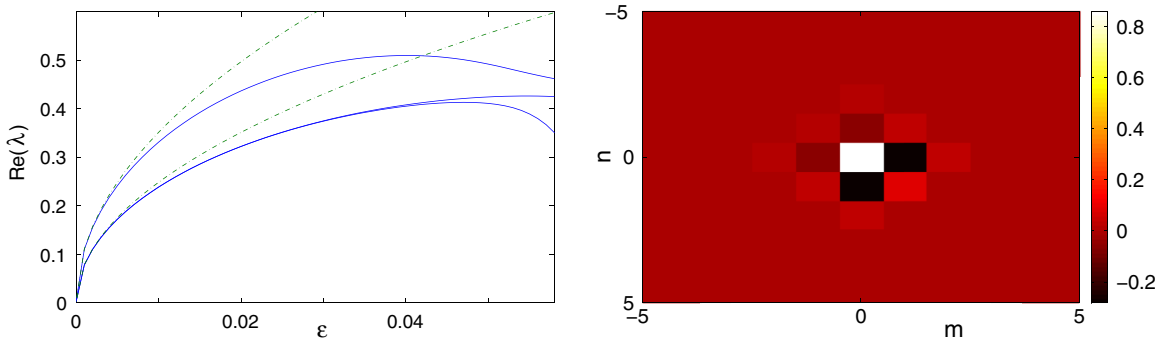

FIG. 6. (Color online) Similar to the previous figures, but now for the four-site, out-of-phase excitation. The left panel shows the numerical result (the blue solid line) and the analytical prediction (the green dash-dotted line) for the three pairs bifurcating from the origin towards the real axis, rendering the configuration highly unstable. A typical example of the configuration profile for $\varepsilon = 0.055$ is shown in the right panel.

Finally, we consider the extended state in which all the sites of the lattice are excited in accordance with the TFA, $v_{m,n} = \sqrt{\mu/g(m,n)}$ [see Eq. (6)]. First, assuming that the coupling constant ε is small, Eqs. (6) and (2) readily yield the leading order correction to the TFA, which, by itself, corresponds to $\varepsilon = 0$ (recall the chemical potential is fixed as $\mu = 1$):

$$v_{m,n} \approx v^{(0)}_{m,n} + \varepsilon v^{(1)}_{m,n} = e^{-(|m|+|n|)} - (\varepsilon/2)\Delta_2(e^{-(|m|+|n|)}). \quad (16)$$

In particular, the accordingly predicted amplitude of the extended mode, at $m = n = 0$, is

$$A_{\max} = 1 - 2(1 - e^{-1})\varepsilon \approx 1 - 1.264\varepsilon. \quad (17)$$

By means of our numerical continuation, it was possible to follow this solution for all the values of the coupling that we considered, up to $\varepsilon = 0.2$. As can be seen in the left panel of the figure, the dependence of the amplitude of the solution on the coupling constant is almost exactly approximated by $A_{\max} = 1 - (5/4)\varepsilon$, i.e., the perturbative result (17) predicts the dependence very accurately. An example of a numerically determined profile of the mode is shown in the right panel of Fig. 9 for $\varepsilon = 0.2$. Furthermore, the numerical analysis has demonstrated that the solution is stable throughout its entire existence interval (up to $\varepsilon = 0.2$; the numerical solution was not extended to large values of ε). Notice that here the

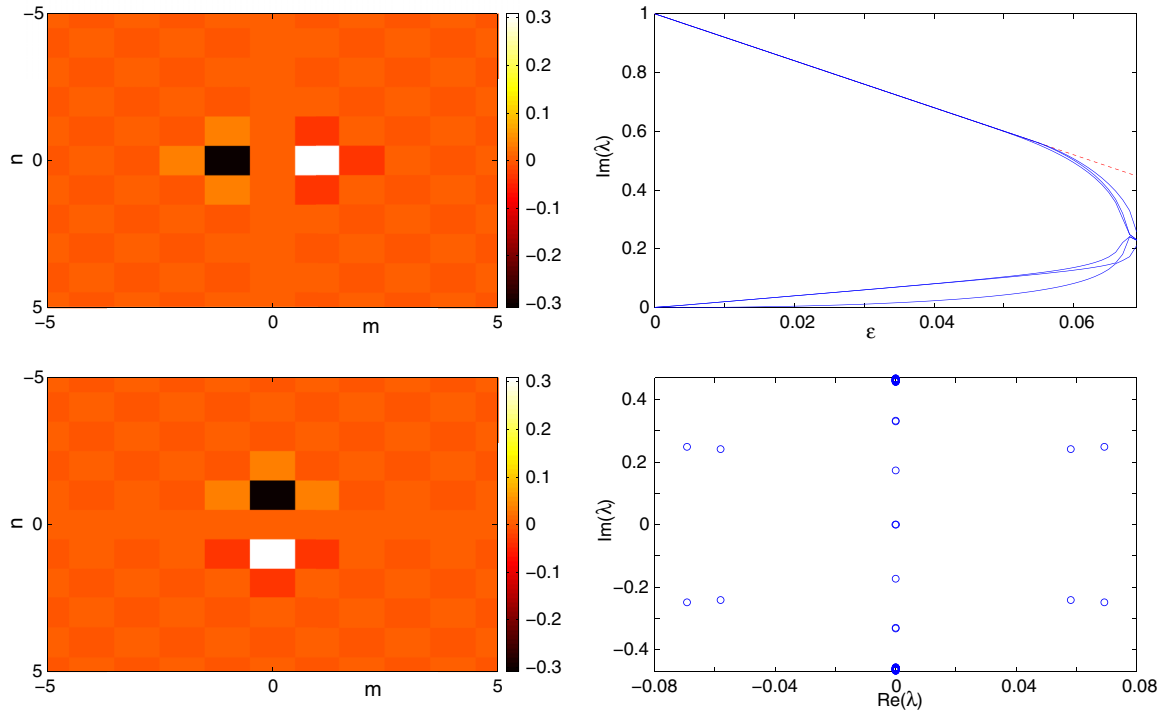

FIG. 7. (Color online) The left panels of the figure illustrate the real (top) and imaginary (bottom) parts of the spatial distribution of a two-dimensional vortex cross. The phases of the four excited sites are 0, $\pi/2$, π, and $3\pi/2$, so that a phase circulation of 2π is achieved when moving along a contour surrounding the mode's pivot. The solution is shown for $\varepsilon = 0.068$, and its corresponding spectral plane is displayed in the bottom right panel. The top right panel illustrates the $O(\varepsilon)$ (or weaker; see the smallest eigenvalue pair) dependence for small ε of the eigenvalue pairs bifurcating from the origin. It is the collision of these pairs with the ones bifurcating from the band edge (which is depicted, as before, by the dashed red line), that leads to the instability at $\varepsilon \geqslant 0.068$.

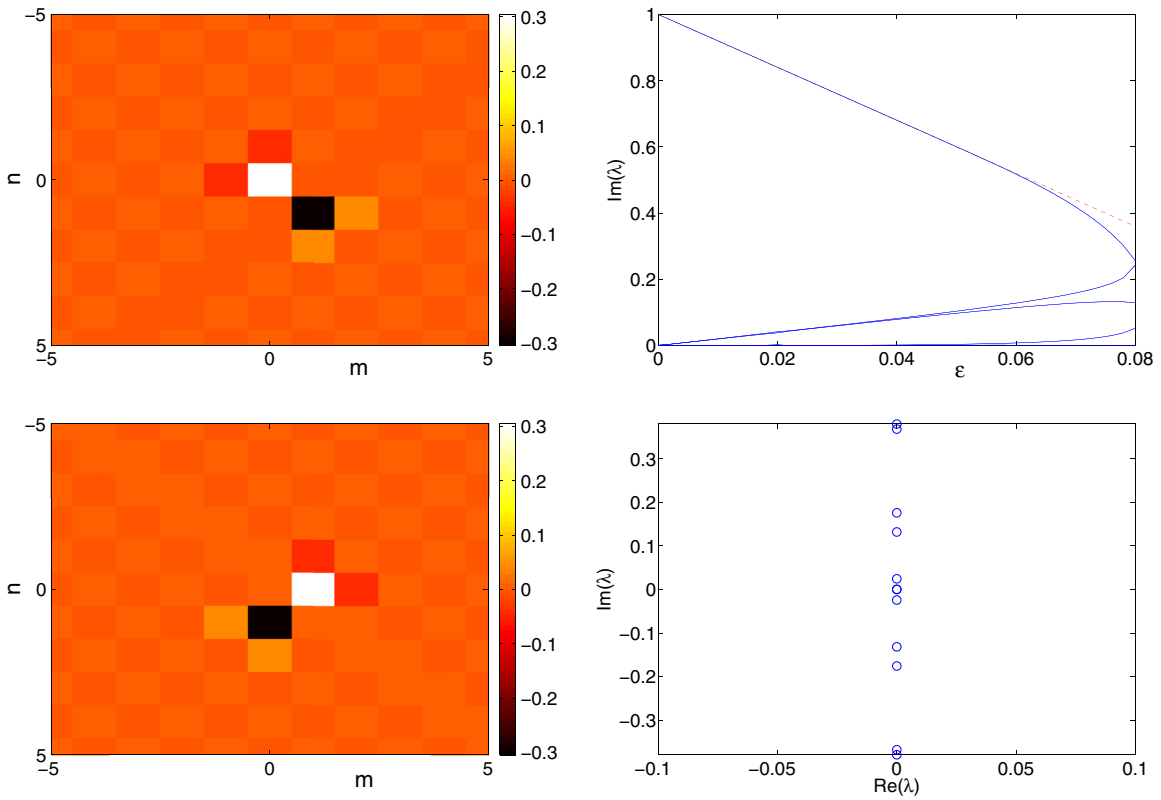

FIG. 8. (Color online) Same as the above figure, but now for a vortex square in the case of a nonlinearity profile symmetric around (0.5,0.5) in the form of Eq. (8). The top left panel (real part) and bottom left panel (imaginary part of the solution), as well as the spectral plane of the bottom right panel are given for $\varepsilon = 0.074$. The top right panel illustrates the trajectory of the imaginary part of the eigenvalues associated with the stability of the configuration up to $\varepsilon \approx 0.08$.

constraint due to potential collision of eigenvalues stemming from the origin and from the continuous spectrum does *not* exist, as actually all eigenvalue pairs bifurcate from the origin along the imaginary axis.

B. Evolution of unstable modes

We now turn to direct numerical simulations of various unstable states. Given that the single-site excitation is stable throughout its domain of existence, we start with the two-site in-phase configuration in Fig. 10. The top left panel of the figure shows the final profile of the solution produced by simulations at $t = 600$, for $\varepsilon = 0.079$. The initial condition is the mode from Fig. 3, weakly perturbed by a multiplicative small-amplitude random perturbation, intended to initiate the instability. The bottom left panel shows the difference between the initial and final profiles, illustrating how the instability expands across the solution. The right panels of the figure show the evolution at the central and adjacent sites, corroborating the same picture. Also evident in the latter is the oscillatory character of the instability associated with this solution.

The evolution of the out-of-phase two-site state for $\varepsilon = 0.07$ is shown in Fig. 11. The top left panel displays the profile

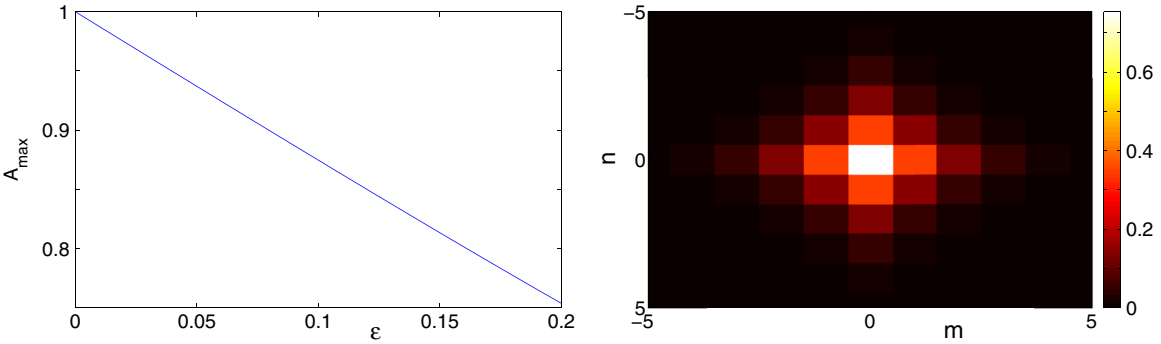

FIG. 9. (Color online) The left panel of the figure shows the dependence of the amplitude of the extended solution on ε, while the right panel displays a typical profile of the extended mode for $\varepsilon = 0.2$.

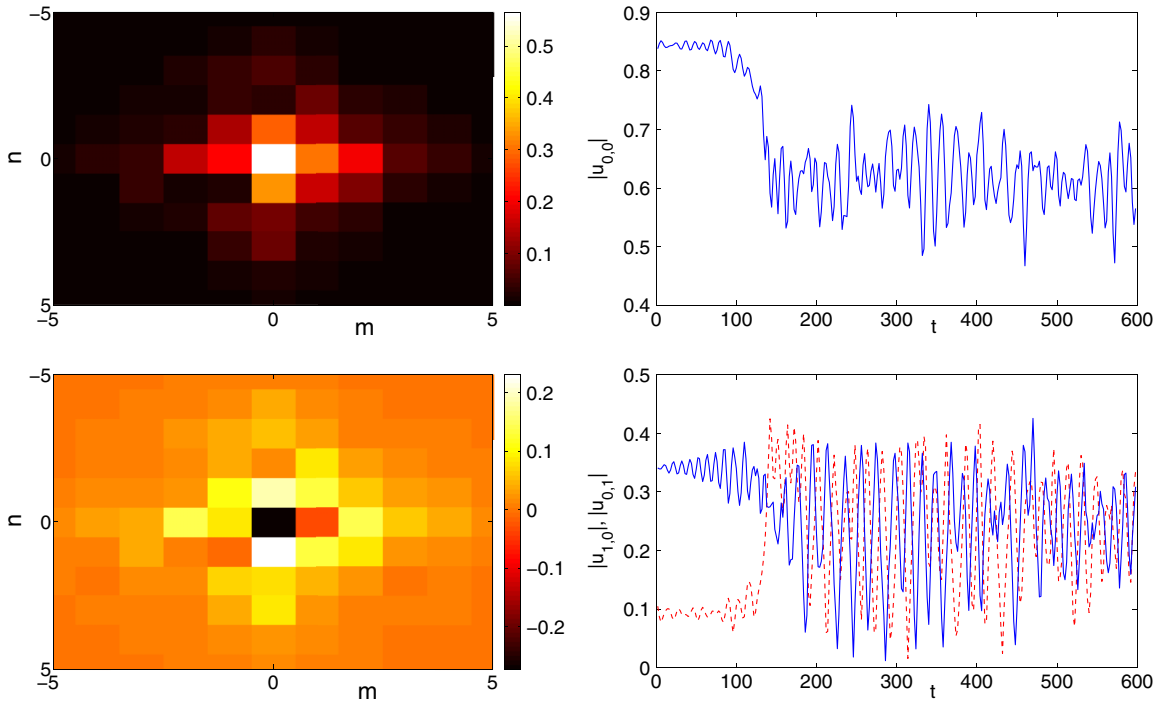

FIG. 10. (Color online) Evolution of the unstable two-site, in-phase mode at $\varepsilon = 0.079$. The top left panel shows the final profile of the absolute value of the discrete wave form at the final simulation time of $t = 600$, while the bottom left panel shows the difference between absolute values of the top left profile and the initial one. The right panels show the absolute value at the central site (top) and at two adjacent ones (bottom); the blue solid line corresponds to the initially excited (1,0) site, and the red dashed line to the (0,1) site.

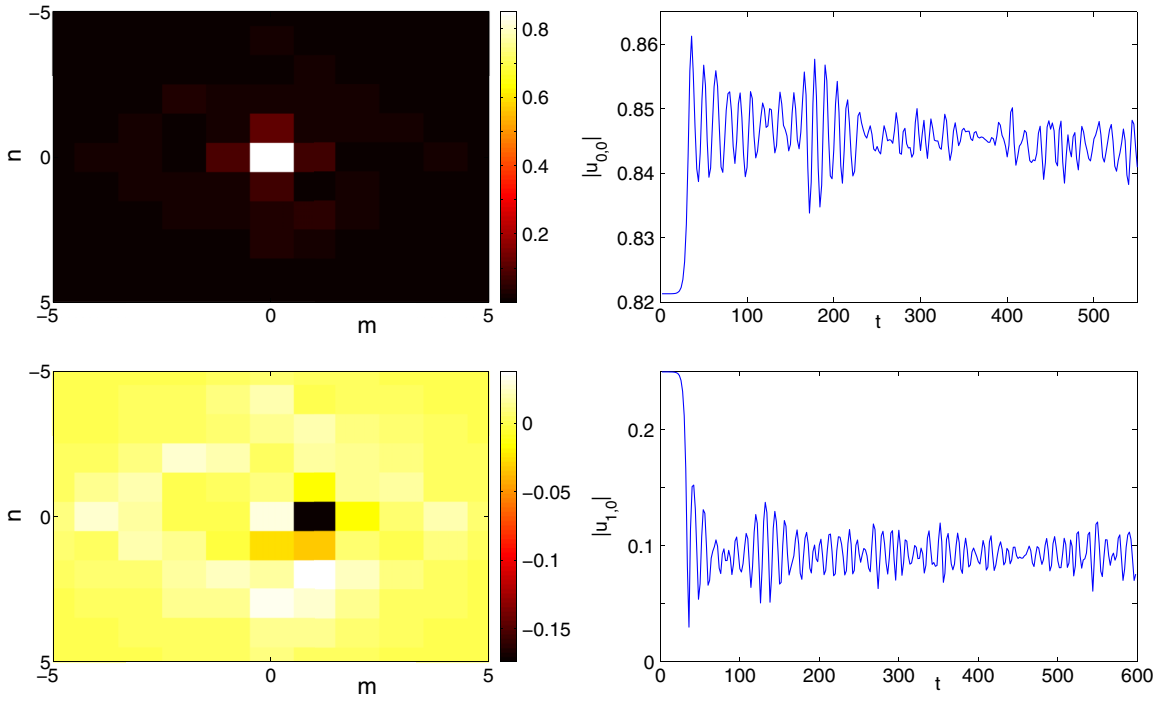

FIG. 11. (Color online) Similar to the previous figure but now for the out-of-phase two-site configuration at $\varepsilon = 0.07$. The top left panel shows the result of the evolution at $t = 600$, while the bottom left panel shows its difference from the input, in terms of the absolute value. The right panels illustrate the evolution at the central (top) and nearest-neighbor (1,0) (bottom) sites, demonstrating the exponential nature of the instability.

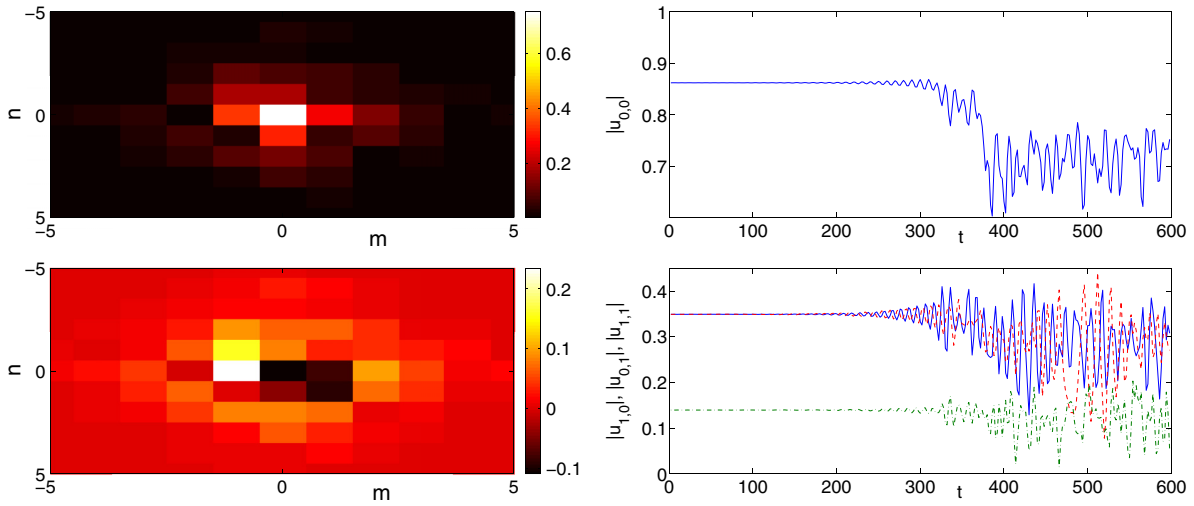

FIG. 12. (Color online) The same as previous figures, but now for the four-site, in-phase excited state with $\varepsilon = 0.075$. Notice the broadening of the solution (left panels) and the oscillatory manifestation of the instability (right panels).

resulting from the dynamics at $t = 600$, while the bottom left panel illustrates the spreading of the solution, through its difference from the initial profile. It is interesting that the structure in the top left panel appears to become more "symmetrized" in the course of the evolution, bearing four nearly symmetric excited sites around the central one. The right panels once again correspond to the evolution of the central site and one of its neighbors. Notice that here, as expected, the growth and manifestation of the instability appear to be exponential, rather than oscillatory.

Moving to the four-site configurations, we explore the instability of the in-phase state at $\varepsilon = 0.075$ in Fig. 12, and of the out-of-phase one at $\varepsilon = 0.055$ in Fig. 13. The former state clearly features (see, especially, the right panels) an oscillatory instability that destroys the configuration, making it broader (see the bottom left panel) and more similar to the configuration with all the sites excited, which is predicted by the TFA; see Eq. (6) (and the top left panel).

On the other hand, the out-of-phase four-site state with $\varepsilon = 0.055$, shown in Fig. 13, illustrates an exponential growth, as illustrated in the right panels of the figure. Here, too, the solution becomes more extended (see, e.g., the bottom left panel), while its central amplitude increases, as shown in the top left and top right panels.

Lastly, the evolution of the vortex configuration from Fig. 7 is displayed in Fig. 14. This configuration, too, is apparently destroyed by the oscillatory instability. The latter leads to a breaking of the symmetry of the amplitude pattern built of the four sites which constitute the vortex (the bottom right panel), as well as to populating the central site (the top right panel), which has identically zero amplitude in exact vortex solutions. The latter effect attests to the destruction of the vorticity, as is confirmed by the top left panel, which shows that the norm of the configuration (for the present case of $\varepsilon = 0.068$) is spread over multiple sites surrounding the central ones. This is also evident from the difference plot (between absolute values of

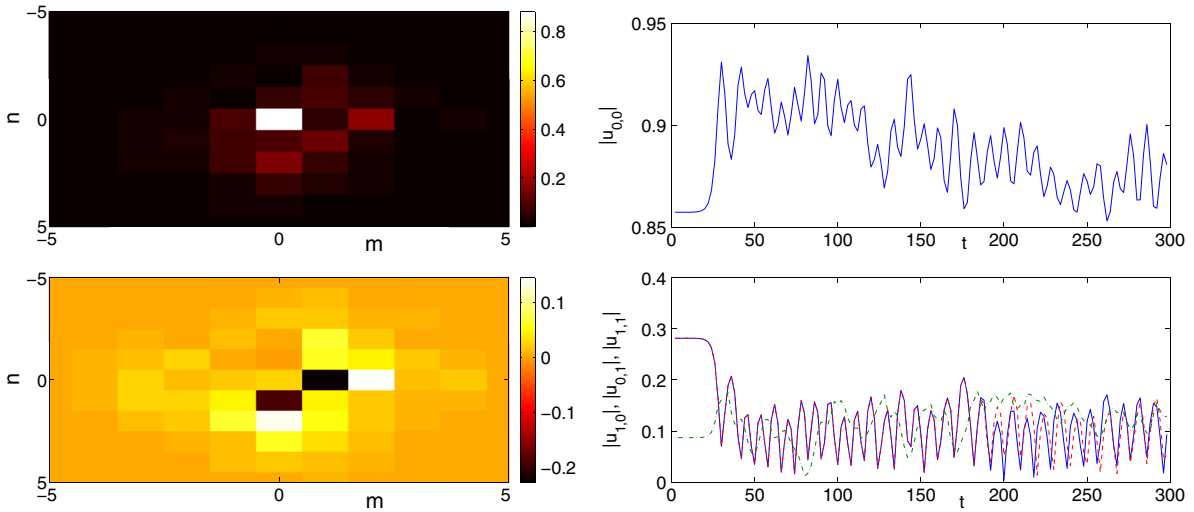

FIG. 13. (Color online) The same as previous figures, but for the exponential instability dominating the dynamics of an out-of-phase configuration at $\varepsilon = 0.055$.

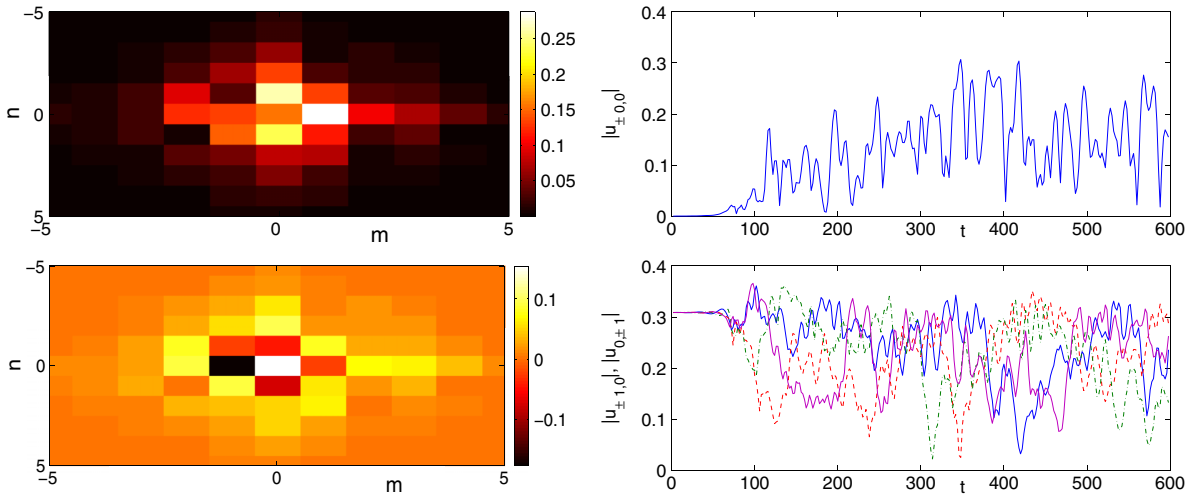

FIG. 14. (Color online) The same as previous figures, but for the vortex with $\varepsilon = 0.068$. The top right panel shows populating the originally empty central site, while the four sites surrounding it no longer carry equal amplitudes, in the course of the development of the oscillatory instability (the bottom right panel).

the initial and the final configurations) presented in the bottom left panel.

IV. CONCLUSIONS AND FUTURE CHALLENGES

In the present work we have explored the existence, stability, and dynamics of different bright solitary waves, as well as vortex configurations, in the 2D defocusing nonlinear Schrödinger lattice with a spatially modulated nonlinearity. The fundamental modification of the present setup enabling the existence of such states is the introduction of the spatially modulated nonlinearity profile, with the local strength growing from the center to the periphery faster than the squared distance. As a result, single-site, two-site (in- or out-of-phase), and four-site (in-, out- or with mixed-phase) configurations have been systematically constructed near the anticontinuum limit. A significant advantage of this construction is not only its full controllability in this limit, but also the ability to analyze the linear stability of the configurations. Going beyond these simplest few-site constructions, we have also explored a vortex cross, as well as the "extended" solution, in which all the sites of the lattice are excited. In fact, solely this last solution was previously identified in the 1D version of the discrete system [15]. Here, this wave form was found to be the most robust one, being stable in the entire parametric region that was considered. All solutions with out-of-phase structures feature instabilities accounted for by real eigenvalue pairs, while in-phase, few-site states are subject to oscillatory instabilities, caused by the collision of imaginary eigenvalue pairs with the continuous spectrum or eigenvalue pairs bifurcating from the edge of the continuous-spectrum band. Monitoring the evolution of the unstable modes, we observed a trend of the norm to spread over multiple sites surrounding the center, and also an apparent tendency to rearrange into a structure reminiscent of the stable extended solution.

There are numerous questions that merit further investigation in this nascent field. Gaining a more systematic understanding, possibly through analytical considerations, of vortex crosses and of vortex squares (e.g., of their eigenvalue dependencies and a potential proof of the symmetry conditions for their existence) are relevant directions. Moreover, detailed stability analysis of the extended bright discrete-soliton configuration should be interesting in its own right. Extending the present configuration to the 3D setting (see Ref. [39]) is another challenging issue. On the other hand, the extension of the study of quantum solitons in the Bose-Hubbard counterpart of the present setting from the 1D setting [17] to 2D is challenging but certainly interesting. Some of these topics are currently under study and results will be reported elsewhere.

ACKNOWLEDGMENTS

The work of D.J.F. was partially supported by the Special Account for Research Grants of the University of Athens. P.G.K. gratefully acknowledges the support of NSF-DMS-1312856, as well as from the US-AFOSR under Grant No. FA950-12-1-0332, and the ERC under FP7, Marie Curie Actions, People, International Research Staff Exchange Scheme (Grant No. IRSES-605096). P.G.K. and B.A.M. gratefully acknowledge the support of the BSF under Grant No. 2010239. This work was supported in part by the US Department of Energy.

[1] Y. V. Kartashov, B. A. Malomed, and L. Torner, Rev. Mod. Phys. **83**, 247 (2011).

[2] M. J. Ablowitz, B. Prinari, and A. D. Trubatch, *Discrete and Continuous Nonlinear Schrödinger Systems* (Cambridge University Press, Cambridge, 2004).

[3] Yu. S. Kivshar and G. P. Agrawal, *Optical Solitons: From Fibers to Photonic Crystals* (Academic, San Diego, 2003).

[4] P. G. Kevrekidis, D. J. Frantzeskakis, and R. Carretero-González, *Emergent Nonlinear Phenomena in Bose-Einstein Condensates: Theory and Experiment* (Springer-Verlag,

Heidelberg, 2008); R. Carretero-González, D. J. Frantzeskakis, and P. G. Kevrekidis, Nonlinearity **21**, R139 (2008); D. J. Frantzeskakis, J. Phys. A: Math. Theor. **43**, 213001 (2010).
[5] O. V. Borovkova, Y. V. Kartashov, L. Torner, and B. A. Malomed, Phys. Rev. E **84**, 035602(R) (2011); O. V. Borovkova, Y. V. Kartashov, B. A. Malomed, and L. Torner, Opt. Lett. **36**, 3088 (2011).
[6] Y. V. Kartashov, V. A. Vysloukh, L. Torner, and B. A. Malomed, Opt. Lett. **36**, 4587 (2011).
[7] O. V. Borovkova, Y. V. Kartashov, V. A. Vysloukh, V. E. Lobanov, B. A. Malomed, and L. Torner, Opt. Express **20**, 2657 (2012).
[8] B. A. Malomed and D. E. Pelinovsky, Appl. Math. Lett. **40**, 45 (2015).
[9] V. E. Lobanov, O. V. Borovkova, Y. V. Kartashov, B. A. Malomed, and L. Torner, Opt. Lett. **37**, 1799 (2012).
[10] J. Zeng and B. A. Malomed, Phys. Rev. E **86**, 036607 (2012).
[11] Y. V. Kartashov, V. E. Lobanov, B. A. Malomed, and L. Torner, Opt. Lett. **37**, 5000 (2012).
[12] Luis E. Young-S., L. Salasnich, and B. A. Malomed, Phys. Rev. A **87**, 043603 (2013).
[13] R. Kishor Kumar, P. Muruganandam, and B. A. Malomed, J. Phys. B: At. Mol. Opt. Phys. **46**, 175302 (2013).
[14] Y. He and B. A. Malomed, Phys. Rev. A **87**, 053812 (2013); Y. Li, J. Liu, W. Pang, and B. A. Malomed, *ibid.* **88**, 053630 (2013).
[15] G. Gligorić, A. Maluckov, L. Hadzievski, and B. A. Malomed, Phys. Rev. E **88**, 032905 (2013).
[16] R. Driben, Y. V. Kartashov, B. A. Malomed, T. Meier, and L. Torner, Phys. Rev. Lett. **112**, 020404 (2014); New J. Phys. **16**, 063035 (2014); Y. V. Kartashov, B. A. Malomed, Y. Shnir, and L. Torner, Phys. Rev. Lett. **113**, 264101 (2014).
[17] L. Barbiero, B. A. Malomed, and L. Salasnich, Phys. Rev. A **90**, 063611 (2014).
[18] P. G. Kevrekidis, *The Discrete Nonlinear Schrödinger Equation* (Springer-Verlag, Heidelberg, 2009).
[19] D. N. Christodoulides, F. Lederer, and Y. Silberberg, Nature (London) **424**, 817 (2003); A. A. Sukhorukov, Y. S. Kivshar, H. S. Eisenberg, and Y. Silberberg, IEEE J. Quantum Electron. **39**, 31 (2003).
[20] F. Lederer, G. I. Stegeman, D. N. Christodoulides, G. Assanto, M. Segev, and Y. Silberberg, Phys. Rep. **463**, 1 (2008).
[21] O. Morsch and M. Oberthaler, Rev. Mod. Phys. **78**, 179 (2006).
[22] M. Peyrard, Nonlinearity **17**, R1 (2004).
[23] N. Boechler, G. Theocharis, S. Job, P. G. Kevrekidis, M. A. Porter, and C. Daraio, Phys. Rev. Lett. **104**, 244302 (2010).
[24] C. Chong, F. Li, J. Yang, M. O. Williams, I. G. Kevrekidis, P. G. Kevrekidis, and C. Daraio, Phys. Rev. E **89**, 032924 (2014).
[25] A. K. Sieradzan, A. Niemi, and X. Peng, Phys. Rev. E **90**, 062717 (2014).
[26] R. S. MacKay and S. Aubry, Nonlinearity **7**, 1623 (1994).
[27] M. Johansson, S. Aubry, Yu. B. Gaididei, P. L. Christiansen, and K. Ø. Rasmussen, Physica D (Amsterdam, Neth.) **119**, 115 (1998).
[28] B. A. Malomed and P. G. Kevrekidis, Phys. Rev. E **64**, 026601 (2001).
[29] D. N. Neshev, T. J. Alexander, E. A. Ostrovskaya, Yu. S. Kivshar, H. Martin, I. Makasyuk, and Z. Chen, Phys. Rev. Lett. **92**, 123903 (2004).
[30] J. W. Fleischer, G. Bartal, O. Cohen, O. Manela, M. Segev, J. Hudock, and D. N. Christodoulides, Phys. Rev. Lett. **92**, 123904 (2004).
[31] D. E. Pelinovsky, P. G. Kevrekidis, and D. J. Frantzeskakis, Physica D (Amsterdam, Neth.) **212**, 1 (2005).
[32] D. E. Pelinovsky, P. G. Kevrekidis, and D. J. Frantzeskakis, Physica D (Amsterdam, Neth.) **212**, 20 (2005).
[33] E. Smirnov, C. E. Rüter, M. Stepić, D. Kip, and V. Shandarov, Phys. Rev. E **74**, 065601(R) (2006).
[34] R. A. Vicencio, E. Smirnov, C. E. Rüter, D. Kip, and M. Stepić, Phys. Rev. A **76**, 033816 (2007).
[35] R. Dong, C. E. Rüter, D. Kip, J. Cuevas, P. G. Kevrekidis, D. Song, and J. Xu, Phys. Rev. A **83**, 063816 (2011).
[36] A. Trombettoni and A. Smerzi, Phys. Rev. Lett. **86**, 2353 (2001).
[37] G. L. Alfimov, P. G. Kevrekidis, V. V. Konotop, and M. Salerno, Phys. Rev. E **66**, 046608 (2002).
[38] H. Sakaguchi and B. A. Malomed, Phys. Rev. A **81**, 013624 (2010).
[39] M. Lukas, D. E. Pelinovsky, and P. G. Kevrekidis, Physica D (Amsterdam, Neth.) **237**, 339 (2008).
[40] P. G. Kevrekidis, H. Susanto, and Z. Chen, Phys. Rev. E **74**, 066606 (2006).